Supplementary

Appendix A Prediction results at lesion-level

Table A1 reports the prediction performance at lesion-level on FAME2 and FCL dataset derived from different models.

Table A1 Prediction performance on FAME2 and FCL dataset derived from different models. DS: diameter stenosis. FFR: fractional flow reserve. LR: Logistic Regression. DeTr: Decision Tree.

Dataset	Model	Accuracy	Recall	Precision	F1	Spec	AUC
FAME2	DS	0.55	0.68	0.37	0.48	0.49	0.59
	FFR	0.59	**0.84**	0.42	0.56	0.49	0.67
	XGBoost	0.69±0.02	0.28±0.04	0.32±0.04	0.30±0.04	0.81±0.02	0.55±0.02
	SVM	0.75±0.02	0.09±0.05	0.37±0.10	0.14±0.06	**0.95±0.03**	0.52±0.02
	LR	**0.76±0.01**	0.05±0.04	0.29±0.25	0.28±0.40	0.92±0.11	0.51±0.02
	DeTr	0.65±0.01	0.39±0.05	0.30±0.04	0.34±0.04	0.72±0.02	0.56±0.02
	ResNet	0.61±0.05	0.59±0.09	0.38±0.02	0.46±0.03	0.62±0.09	0.61±0.03
	GLE	0.69±0.02	0.72±0.04	**0.49±0.06**	**0.58±0.05**	0.68±0.03	**0.71±0.02**
FCL	DS	0.62	0.13	0.75	0.22	0.97	0.55
	FFR	0.60	0.04	**0.99**	0.08	**0.99**	0.52
	XGBoost	0.60±0.05	0.47±0.13	0.54±0.07	0.50±0.11	0.71±0.06	0.61±0.11
	SVM	0.59±0.03	0.19±0.09	0.50±0.15	0.27±0.12	0.88±0.06	0.53±0.03
	LR	0.55±0.03	0.17±0.04	0.46±0.12	0.23±0.04	0.84±0.10	0.50±0.02
	DeTr	0.62±0.08	0.52±0.19	0.54±0.10	0.53±0.14	0.69±0.04	0.60±0.09
	ResNet	0.69±0.04	**0.72±0.07**	0.63±0.08	0.67±0.02	0.68±0.10	0.70±0.03
	GLE	**0.76±0.05**	0.70±0.06	0.71±0.07	**0.70±0.01**	0.78±0.12	**0.73±0.05**

Appendix B Prediction results at patient-level

Table B2 summarizes the prediction performance at patient-level on FAME2.

Table B2 Patient-level prediction results on FAME2 dataset.

Method	Acc	Recall	Precision	F1	Spec	AUC
FFR	0.57	0.61	0.32	0.42	0.55	0.58
DS	0.47	**0.74**	0.30	0.43	0.38	0.56
MAX	0.68±0.03	0.47±0.04	0.41±0.05	0.44±0.04	**0.76±0.02**	0.62±0.03
MEAN	0.62±0.04	0.59±0.03	0.36±0.04	0.45±0.04	0.63±0.06	0.61±0.02
MA	0.68±0.06	0.61±0.11	0.43±0.02	0.50±0.04	0.70±0.11	0.63±0.02
CMA	**0.71±0.04**	0.67±0.07	**0.46±0.03**	**0.55±0.03**	0.72±0.07	**0.69±0.06**

Appendix C Ablation study on clinically-relevant features

Table C3 summaries the results from an ablation study conducted on clinically-relevant information and its impact on the events prediction performance.

Table C3 Prediction performance without clinically-relevant features on FAME2 and FCL dataset derived from different models . DS: diameter stenosis. FFR: fractional flow reserve. LR: Logistic Regression. DeTr: Decision Tree.

Dataset	Model	Accuracy	Recall	Precision	F1	Spec	AUC
FAME2	XGBoost	0.67±0.01	0.19±0.05	0.24±0.05	0.21±0.04	0.82±0.02	0.51±0.02
	SVM	**0.76±0.02**	0.01±0.01	0.11±0.15	0.02±0.03	**0.99±0.01**	0.50±0.004
	LR	**0.76±0.02**	0.06±0.04	0.38±0.23	0.11±0.07	0.97±0.004	0.52±0.02
	DTr	0.61±0.04	0.26±0.06	0.22±0.05	0.24±0.05	0.72±0.04	0.49±0.04
	ResNet	0.32±0.06	**0.88±0.12**	0.28±0.01	0.42±0.01	0.10±0.11	0.49±0.01
	GLE	0.53±0.02	0.73±0.06	**0.37±0.02**	**0.49±0.02**	0.44±0.06	0.59±0.02
FCL	XGBoost	0.53±0.06	0.40±0.10	0.43±0.08	0.41±0.09	0.62±0.06	0.51±0.06
	SVM	0.54±0.04	0.19±0.09	0.44±0.08	0.24±0.07	**0.80±0.13**	0.49±0.02
	LR	0.54±0.05	0.15±0.06	0.43±0.13	0.21±0.06	0.83±0.09	0.49±0.04
	DTr	0.57±0.08	0.55±0.08	0.49±0.11	0.52±0.09	0.58±0.11	0.56±0.08
	ResNet	0.64±0.04	0.70±0.08	0.56±0.05	0.62±0.03	0.59±0.12	0.65±0.03
	GLE	**0.66±0.07**	**0.73±0.08**	**0.60±0.10**	**0.65±0.03**	0.63±0.17	**0.67±0.05**

Appendix D Graph examples

Figure D1 illustrates three instances of the constructed graphs exhibiting varying node intensities. In this representation, the first two columns depict a raw ICA image alongside corresponding annotations. The last six columns display the point cloud of node coordinates and a graph representation of these points with inner node intensities of 0, 0.5, and 1, respectively. Compared to the raw image, the graph representation of the artery clearly preserves the geometry, while filtering out the pixel noise from the background.

Appendix E Effect of graph node connectivity.

To investigate the effect of the graph connective matrix and its sparsity pattern, we train GLE on the FAME2 dataset using alternate KNN and DT as node connectivity methods, respectively. We test the performance of the algorithm under 5 or 10 neighbors to connect with. Figure E2.a illustrates four graphs constructed using KNN and DT method with different numbers of neighbors. In the case of KNN, K = 5, 10 represent the K nearest neighbours of each node with respect to the spatial proximity that is approximated by the Euclidean distance. While in the DT method, the values of 5 and 10 the maximum euclidean distance that is allowed for a connection to be preserved. The prediction performance derived from GLE in Figure E2.b reveals that DT approach outperforms KNN overall, yielding better results in term of Acc, Prec, F1, Spec and AUC. Although DT-10 achieved higher Acc, Spec and AUC, DT-5

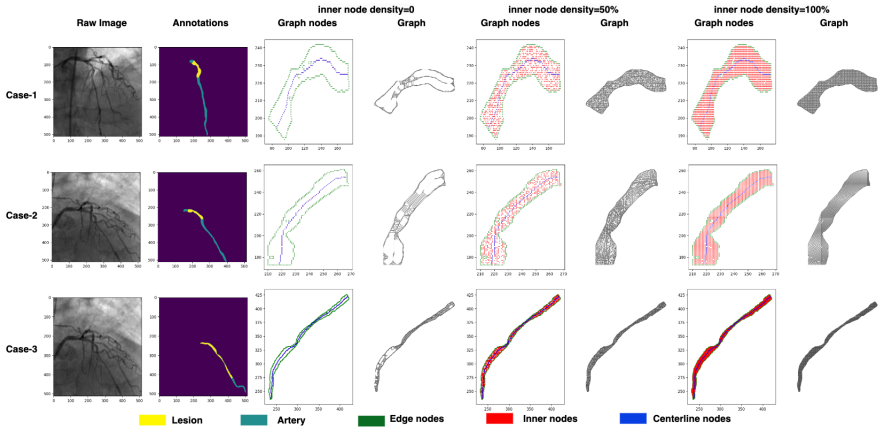

Fig. D1 Graph constructed from examples of ICA images. Each example shows three graphs constructed using three different inner node intensities of 0, 50% and 100%, respectively.

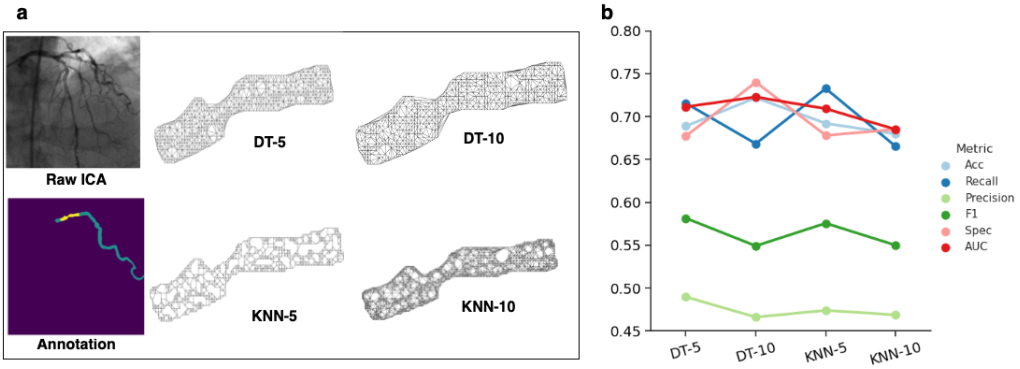

Fig. E2 Graph construction examples and the results of ablation study on the graph node connectivity. **a.** An example of graph constructed using K-nearest neighbors (KNN) and Delaunay triangulation (DT) with different numbers of neighbors. **b.** Prediction performance derived from each node connectivity methods.

show the best performance with Prec and F1. Therefore, DT-5 is selected as the graph construction method in this work. More detailed results are listed in Table E4.

Table E4 Impact of node connectivity algorithms on the prediction performance on FAME2 dataset. DT: Delaunay triangulation. NC: node connectivity algorithms. The number of 5 and 10 mean closer neighbors to connect with, for KNN, and the max euclidean distance that is allowed to be retained for Delaunay triangulation.

NC	Acc	Rec	Prec	F1	Spec	AUC
DT-5	0.69±0.02	0.72±0.04	**0.49±0.06**	**0.58±0.05**	0.68±0.03	0.71±0.02
DT-10	**0.72±0.05**	0.67±0.01	0.47±0.06	0.55±0.02	**0.74±0.08**	**0.73±0.03**
KNN-5	0.69±0.04	**0.73±0.04**	0.47±0.03	0.57±0.03	0.68±0.05	0.71±0.03
KNN-10	0.68±0.06	0.66±0.06	0.47±0.05	0.55±0.03	0.68±0.09	0.68±0.04